Supporting Information

Electrophoretic deposition as a new approach to produce optical sensing films adaptable to microdevices

M. Marín-Suárez[a]*, S. Medina-Rodríguez [a,b], O. Ergeneman[c]*, S. Pané[c], J.F. Fernández-Sánchez[a], B. J. Nelson[c], A. Fernández-Gutiérrez[a]

[a]Department of Analytical Chemistry, Faculty of Sciences, University of Granada, Avda. Fuentenueva s/n, E-18071 Granada, Spain

[b]Department of Signal Theory, Networking and Communications, CITIC-UGR, University of Granada, C/ Periodista Rafael Gómez 2, E-18071 Granada, Spain

[c]Institute of Robotics and Intelligent Systems, ETH Zurich, Tannenstrasse 3, CH-8092 Zurich, Switzerland

*Corresponding author: Tel.: +34 958248593. *E-mail address: mmarinst@ugr.es (*M. Marín-Suárez*)* oergeneman@ethz.ch (O. Ergeneman)

Index:

- Phase-resolved method
- Description of the measurement setup.
- Selection of the optimal modulation frequency.

Figures:

Figure ESI-1. Schematic diagram of the designed experimental setup for phase-shift measurements.

Figure ESI-2. Selection of the modulation frequency.

Figure ESI-3. Luminescence spectra of PtTFPP nanoparticles deposited electrophoretically.

Figure ESI-4. Hamaker calculations

Figure ESI-5. Phase shift measurement and decay plot.

Figure ESI-6. Stern-Volmer plots of the sensing films obtained for the different time of deposition for 40 and 30 V cm^{-1}.

Figure ESI-7. Stern-Volmer plots of the sensing films obtained for the different time of deposition for 20 and 10 V cm^{-1}.
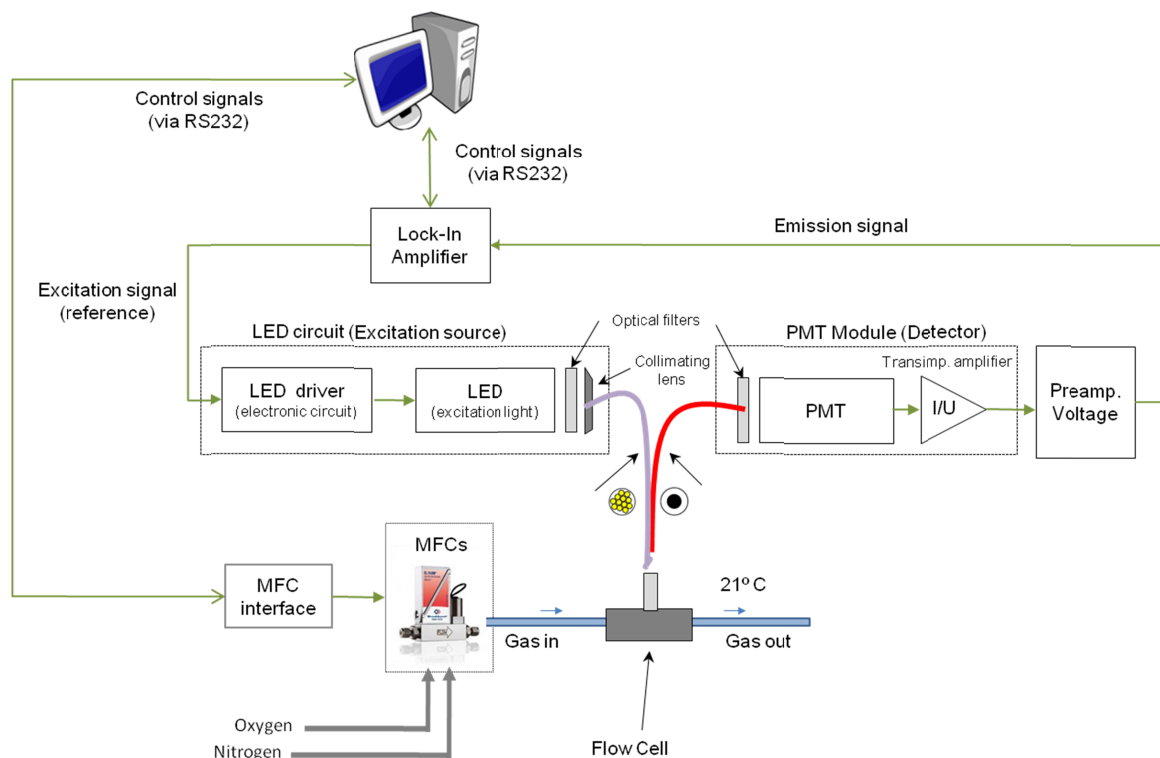
Phase-resolved method

Luminescence sensing can be performed in different ways: recording either emission intensity or lifetime at different oxygen concentrations.[1] Recording intensity of luminescence [1,2] is relatively simple and accurate in the laboratory, but highly dependent on the external perturbations. [1,3] These problems can be minimized by measuring the lifetime (τ) of the oxygen-sensitive layers for different oxygen concentrations.[4] The lifetime of emission can be measured either in the time domain or in the frequency domain.[1] Time-domain measurements are ideally suited to eliminate background luminescence and scattering,[5] but they usually require more sophisticated instrumentation than frequency-domain sensing.[3,6]

In this work, a phase-resolved method (in the frequency-domain) was selected to determine the oxygen sensitivity of the layers. The sensing layer was excited with a sinusoidally modulated light that consequently causes a modulated emission at the identical frequency. Because of the lifetime of the indicator dye, this emission exhibits a time delay (i.e. phase shift) respect to the excitation signal. Both the phase shift (Φ) and the amplitude, (named here as magnitude, R), of the modulated emission signal with respect to the excitation signal is measured using a commercial dual-phase lock-in amplifier and can be used to evaluate the oxygen sensitivity. [1,3] However, for practical applications, the phase-shift measurement is preferred due to the fact that the magnitude (as it happens in the intensity-based measurements), is strongly affected by variable level of background lights (among others).

The input excitation signal is used as a reference to establish the zero-phase position, and the lifetime is indirectly obtained by measurement the phase shift between excitation and emission signals.
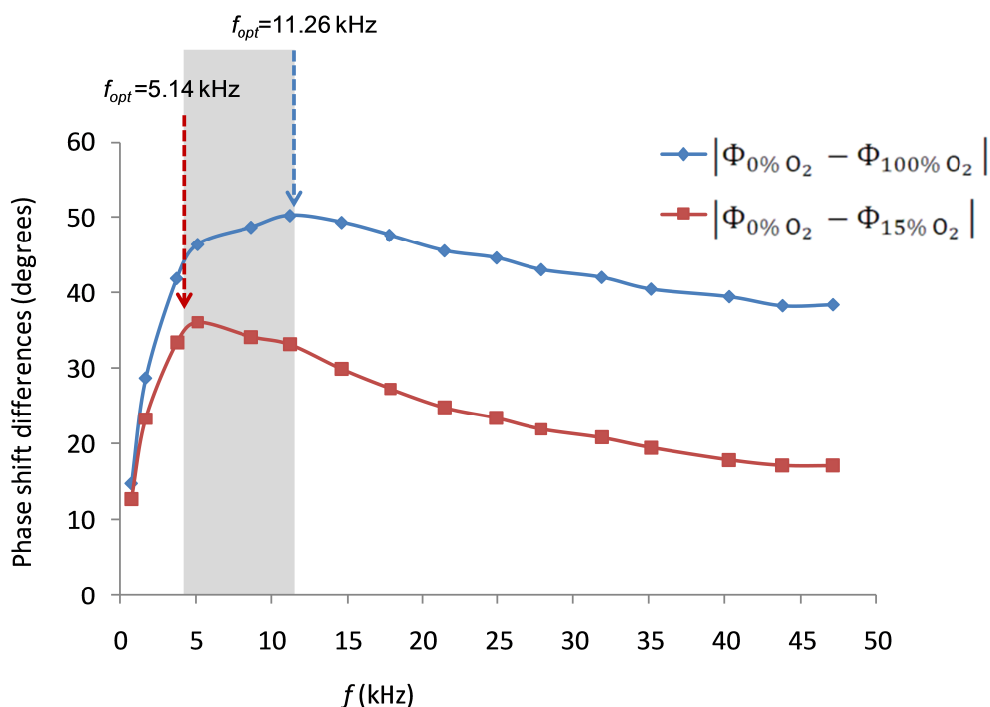
Figures

Control signals
(via RS232)

Control signals
(via RS232)

Lock-In
Amplifier

Emission signal

Excitation signal
(reference)

LED circuit (Excitation source)

Optical filters

Collimating
lens

PMT Module (Detector)

Transimp. amplifier

LED driver
(electronic circuit)

LED
(excitation light)

PMT

I/U

Preamp.
Voltage

MFCs

MFC
interface

21º C

Gas in

Gas out

Oxygen

Nitrogen

Flow Cell

Figure ESI-1. Schematic diagram of the designed experimental setup for phase-shift measurements

Description of the measurement setup

ESI-1 shows a schematic illustration of the setup for the phase shift measurements. An ultraviolet LED (Ocean optics, model LS-450 LED-395, λ_{peak}=395 nm, angle of illumination 15º, LED diameter 5 mm, luminous power 25 µW when coupled into a 600 µm optical fiber core, www.oceanoptics.com) was used as the excitation light source. A sinusoidal signal extracted from the internal signal generator of a dual-phase lock-in amplifier (Stanford Research System, model SR830, www.thinksrs.com) at a fixed frequency of 5145 Hz was used to modulate the current of the LED light source. An

optical bandpass filter (Thorlabs GmbH, model MF390-18, $\lambda_{central}$=390 nm, FWHM=18 nm, www.thorlabs.com) was placed after the UV LED to prevent interference and the light was directly coupled into a bifurcated fiber optic bundle (Avantes Inc., model FCR-7xx200-2, wavelength range 200-800 nm (UV-VIS), 12 ilumnation fibers 200 µm core diameter, 1 read fiber 600 µm core diameter, N.A. 0.22, www.avantes.com). One of the branches of the fiber optic bundle conducted the excitation light to the sensing phase, while the other was used to guide the phase-shifted luminescent emission from the sensing phase to the detector (a photomultiplier tube (PMT) Hamamatsu Photonics Japan, model H10723-20, transimpedance 100 kΩ, BW DC-1 MHz, www.hamamatsu.com). The emission light was previously filtered with an optical bandpass filter (Hamamatsu Photonics Japan, model A10033-03, $\lambda_{central}$=630 nm, FWHM=60 nm) placed before the PMT, in order to separate the reflected excitation light from the emission. The voltage signal provided by the PMT was amplified using a commercial low-noise programmable voltage preamplifier (Stanford Research Systems, model SIM911 BJT), which presented 1.8 nV/$\sqrt{Hz}$ input noise, low output noise, 1 MHz bandwidth and selectable gain from 1 to 100. Finally, the aforementioned dual-phase lock-in amplifier was also used to measure the phase shift between the reference signal and the emission signal emitted by the sensing phase as well as the magnitude of the emission signal.

The additional phase shift introduced by the electronic components[7] (PMT, LED driver, amplifier, etc.) was evaluated using a reference LED (LED Supply, model L2-0-R5TH50-1, λ_{peak}=660 nm, angle of illumination 50º, LED diameter 5 mm, luminous intensity 2000 mcd typ. @ 20mA, www.ledsupply.com).

Figure ESI-2. Effect of the modulation frequency on the phase difference at two oxygen concentrations. Average phase differences ($\left|\Phi_{0\% \, O_2} - \Phi_{x\% \, O_2}\right|$) at low (15%) and high (100%) oxygen concentration at different modulation frequencies, obtained for the sensing films developed by EPD and measured with the setup described in Figure 1. The optimal modulation frequency between 0-30% oxygen is expected to be between 5145 and 11257 Hz.

Selection of the optimal modulation frequency.

The phase-based lifetime measurement at a fixed frequency (f) requires the choice of an optimal modulation frequency.[1] The classical method to obtain the optimal f consists of determining the value where the sensitivity of the phase shift with respect to the lifetime reaches its maximum value, $f_{opt} = 1/2\pi\tau$, which corresponds to a phase shift equal to 45°.[1, 8] However, the selection of optimal modulation frequency also depends on the sensing application. When the maximum dynamic range for the phase shift measurements (and, thus, for the lifetime measurements) want to be achieved, the preferred choice is to adjust the modulation frequency such that the phase difference

between the extremes of the analyte measurement range is maximized. Fig. ESI-2 shows the phase shift differences between 0 and 15% O_2 (as a example for low oxygen concentration), with a maximum at 5145 Hz, and the phase shift differences between 0 and 100% (as representative for high oxygen content) with a maximum at 11259 Hz. From this, it can be derived that the range of optimal modulation frequencies is between 5145 and 11259 Hz for oxygen concentrations higher than 15%.

For the final selection of the modulation frequency it should be also taken into account that the SNR (signal-to-noise ratio) decreases with increasing modulation frequency (i.e., the amplitude of the optical signal (optical power) decreases with increasing of the modulation frequency of the LED).[8] This aspect is of vital importance for practical applications, especially for *in vivo* applications when a weak amount of light reaches the photodetector. Therefore, the selection of the optimal modulation frequency for this kind of measurements was made as a compromise between increased SNR and reduced phase sensitivity for low modulation frequencies[3, 9]. Thus, f was set at the lower value (5145 Hz) which still ensure a wide dynamic range for the phase shift measurement.
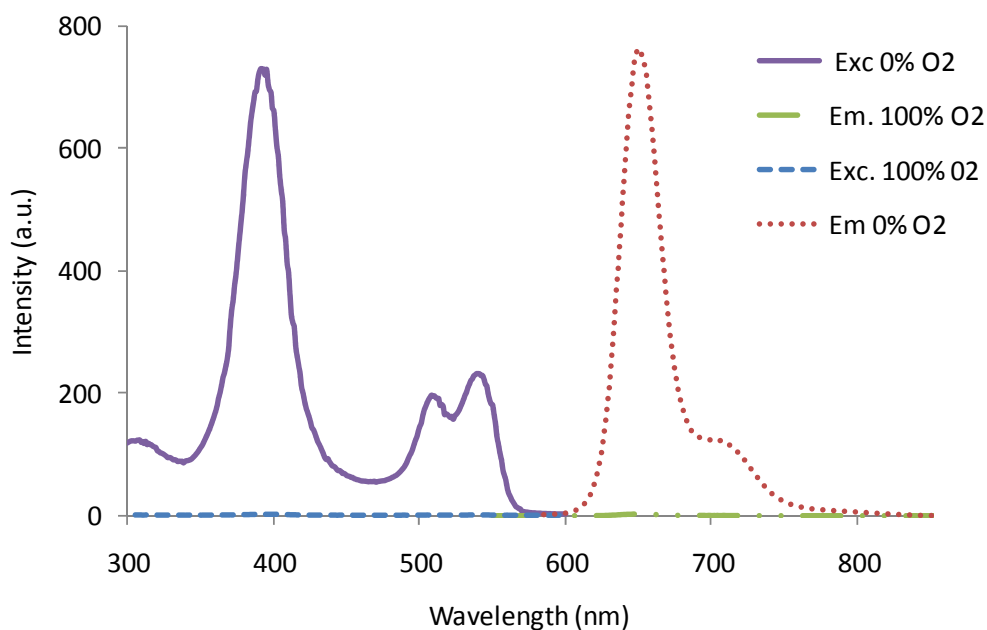
Figure ESI-3. Luminescence spectra of PtTFPP nanoparticles deposited electrophoretically by 40 V cm^{-1} / 1min. Excitation and emission spectra of in the absence of oxygen (purple solid line and red dotted line respectivaly) and in the presence of 100% oxygen. (blue dashed line and green dash-dotted line) slits-width$_{exc/em}$=20/20 nm, delay time=0.1 ms, gate time=5 ms, detector voltage=800 V, total flow-rate 200 mL min^{-1}.
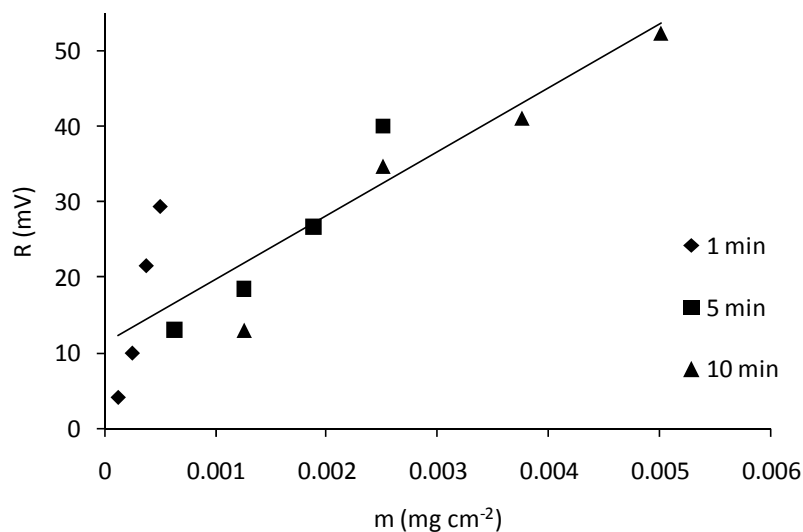
Fig. ESI-4. Relation between the theoretical deposited mass (m) calculated by Hamaker equation and magnitude of the emission signal (R) for all the chips in absence of oxygen.

Calculation of the deposited mass

The model of EPD kinetics proposed by Hamaker in 1940[10, 11] relates the deposited mass, m (mg), with the slurry properties, such as suspension concentration, C_s (mg cm^{-3}) and electrophoretic mobility, μ (cm^2 s^{-1} V^{-1}), as well as with physical and electrical conditions imposed on the system such as electric field, E (V cm^{-1}), deposition area, S (cm^2), and deposition time, t (s) according to equation:

$$m=C_s\mu SEt$$

With this equation and the properties of the dispersión of particles, the theoretical mass deposited by EPD was calculated for each pair of potential and time (see table).

| Cs (mg cm^{-3})	μ (μmcm V^{-1} s^{-1})	E (V cm^{-1})	t (s)	m (mg)
			60	$5.0156 \cdot 10^{-4}$
		40	300	$2.5078 \cdot 10^{-3}$
			600	$5.0156 \cdot 10^{-3}$
			60	$3.7617 \cdot 10^{-4}$
		30	300	$1.8809 \cdot 10^{-3}$
$7.8125 \cdot 10^{-2}$	$2.675 \cdot 10^{-6}$		600	$3.7617 \cdot 10^{-3}$
			60	$2.5078 \cdot 10^{-4}$
		20	300	$1.2539 \cdot 10^{-3}$
			600	$2.5078 \cdot 10^{-3}$
			60	$1.2539 \cdot 10^{-4}$
		10	300	$6.2695 \cdot 10^{-4}$
			600	$1.2539 \cdot 10^{-3}$
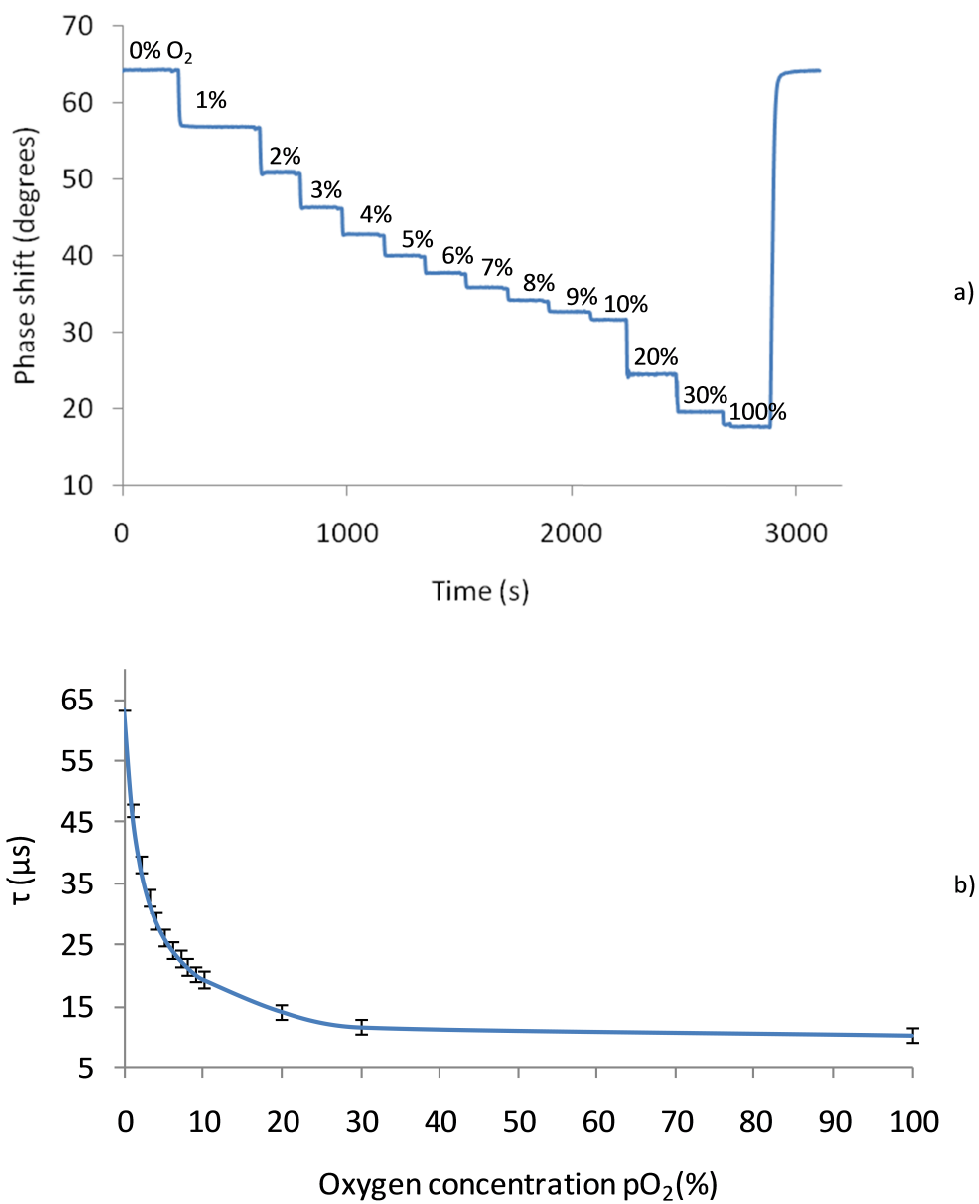
Figure ESI-5. a) Variation of the phase shift and b) decay plot of chip 40 V cm^{-1}/ 1 min under different oxygen concentrations, both obtained with the setup described in ESI-1 (f= 5145 Hz).
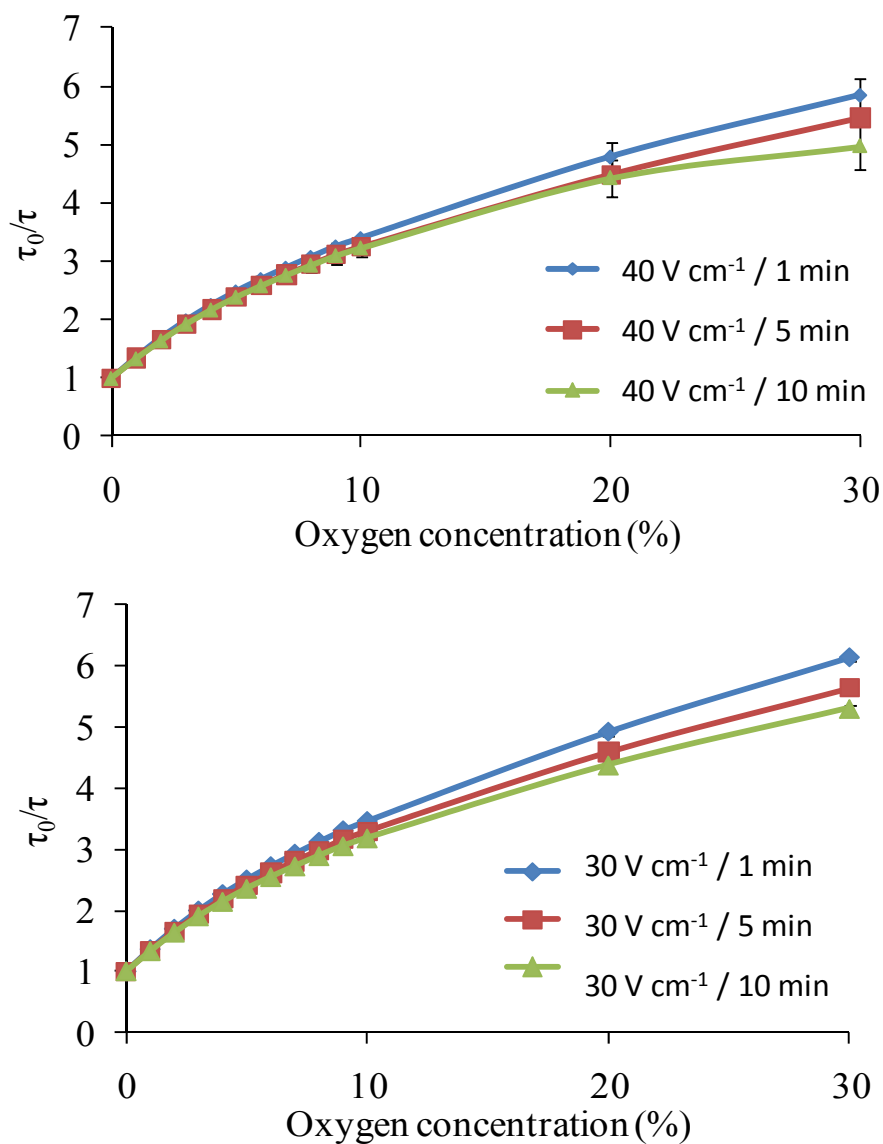
Figure ESI-6. Stern-Volmer plots of for the sensing films obtained via EPD for the different deposition time and an applied potential of a) 40 V cm^{-1}, b) 30 V cm^{-1}. The adjustment was done using Demas model, and the error bars are calculated by the 3 replicas.
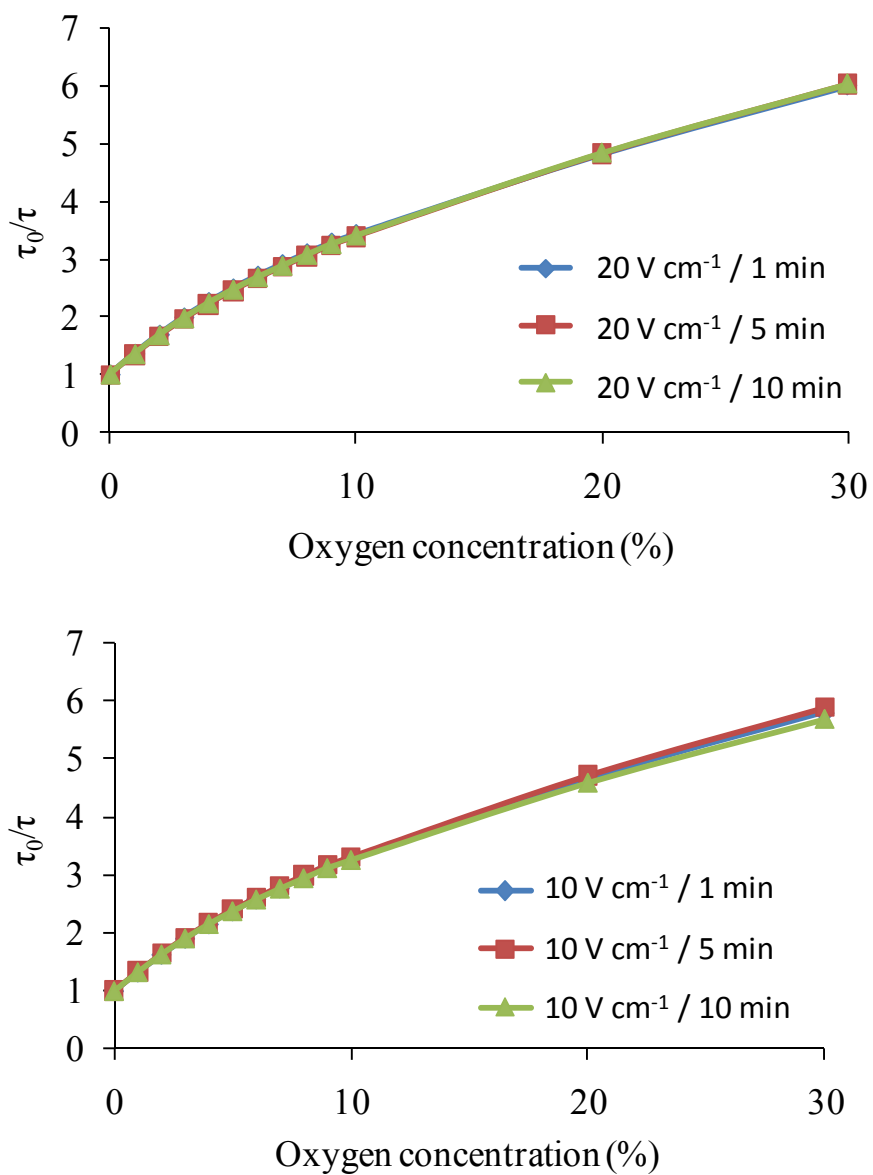
Figure ESI-7. Stern-Volmer plots of for the sensing films obtained via EPD for the different deposition times and an applied potential of a) 20 V cm^{-1}, b) 10 V cm^{-1}. The adjustment was done using Demas model, and the error bars are calculated by the 3 replicas.

References ESI

1. J. R. Lakowicz, *Principles of fluorescence spectroscopy*, Springer2006.
2. M. Marín-Suárezdel Toro, J. F. Fernández-Sánchez, E. Baranoff, M. K. Nazeeruddin, M. Graetzel and A. Fernández-Gutiérrez, *Talanta*, 2010, 82, 620-626.
3. S. Medina-Rodríguez, A. de la Torre-Vega, J. F. Fernández-Sánchez and A. Fernández-Gutiérrez, *Sensors and Actuators B: Chemical*, 2013, 176, 1110-1120.
4. P. Hartmann, M. J. P. Leiner and M. E. Lippitsch, *Sensors and Actuators: B. Chemical*, 1995, 29, 251-257.
5. D. M. Jenkins, C. Zhu and W. W. Su, *Applied Engineering in Agriculture*, 2008, 24, 259-263.
6. W. Trettnak, C. Kolle, F. Reininger, C. Dolezal and P. O'Leary, *Sensors and Actuators B: Chemical*, 1996, 36, 506-512.
7. C. McDonagh, C. Kolle, A. K. McEvoy, D. L. Dowling, A. A. Cafolla, S. J. Cullen and B. D. MacCraith, *Sensors and Actuators B: Chemical*, 2001, 74, 124-130.
8. V. I. Ogurtsov and D. B. Papkovsky, *Sensors and Actuators B: Chemical*, 1998, 51, 377-381.
9. M. Valledor, J. C. Campo, I. Sánchez-Barragán, J. M. Costa-Fernández, J. C. Alvarez and A. Sanz-Medel, *Sensors and Actuators, B: Chemical*, 2006, 113, 249-258.
10. H. C. Hamaker, *Transactions of the Faraday Society*, 1940, 35, 279-287.
11. B. Ferrari and R. Moreno, *Journal of the European Ceramic Society*, 2009, 30, 1069-1078.